Research Article | Vol. 7, No. 12 | 1 Dec 2016 | BIOMEDICAL OPTICS EXPRESS 5129

Biomedical Optics EXPRESS

Raman spectroscopy detects distant invasive brain cancer cells centimeters beyond MRI capability in humans

MICHAEL JERMYN,[1,2,3] JOANNIE DESROCHES,[3] JEANNE MERCIER,[3] KARL ST-ARNAUD,[3] MARIE-CHRISTINE GUIOT,[2,4] FREDERIC LEBLOND,[3,5,6,7] AND KEVIN PETRECCA[2,6,8]

[1]*Thayer School of Engineering, Dartmouth College, 14 Engineering Dr., Hanover, NH 03755, USA*
[2]*Department of Neurology and Neurosurgery, Montreal Neurological Institute and Hospital, McGill University, 3801 University St., Montreal, QC, H3A 2B4, Canada*
[3]*Dept. of Engineering Physics, Polytechnique Montreal, CP 6079, Succ. Centre-Ville, Montreal, QC, H3C 3A7, Canada*
[4]*Division of Neuropathology, Department of Pathology, McGill University, 3801 University St., Montreal, QC, H3A 2B4, Canada*
[5]*Centre de Recherche du Centre Hospitalier de l'Université de Montréal, 900 rue Saint-Denis, H2X 0A9, QC, Canada*
[6]*These authors contributed equally to this work*
[7]*frederic.leblond@polymtl.ca*
[8]*kevin.petrecca@mcgill.ca*

Abstract: Surgical treatment of brain cancer is limited by the inability of current imaging capabilities such as magnetic resonance imaging (MRI) to detect the entirety of this locally invasive cancer. This results in residual cancer cells remaining following surgery, leading to recurrence and death. We demonstrate that intraoperative Raman spectroscopy can detect invasive cancer cells centimeters beyond pathological T1-contrast-enhanced and T2-weighted MRI signals. This intraoperative optical guide can be used to detect invasive cancer cells and minimize post-surgical cancer burden. The detection of distant invasive cancer cells beyond MRI signal has the potential to increase the effectiveness of surgery and directly lengthen patient survival.

OCIS codes: (170.5660) Raman spectroscopy; (170.1610) Clinical applications; (170.6935) Tissue characterization.

References and links

1. K. Petrecca, M.-C. Guiot, V. Panet-Raymond, and L. Souhami, "Failure pattern following complete resection plus radiotherapy and temozolomide is at the resection margin in patients with glioblastoma," J. Neurooncol. **111**(1), 19–23 (2013).
2. W. Stummer, T. Meinel, C. Ewelt, P. Martus, O. Jakobs, J. Felsberg, and G. Reifenberger, "Prospective cohort study of radiotherapy with concomitant and adjuvant temozolomide chemotherapy for glioblastoma patients with no or minimal residual enhancing tumor load after surgery," J. Neurooncol. **108**(1), 89–97 (2012).
3. A. A. Brandes, A. Tosoni, E. Franceschi, M. Reni, G. Gatta, and C. Vecht, "Glioblastoma in adults," Crit. Rev. Oncol. Hematol. **67**(2), 139–152 (2008).
4. M. L. Goodenberger and R. B. Jenkins, "Genetics of adult glioma," Cancer Genet. **205**(12), 613–621 (2012).
5. R. Weissleder and M. J. Pittet, "Imaging in the era of molecular oncology," Nature **452**(7187), 580–589 (2008).
6. M. Jermyn, K. Mok, J. Mercier, J. Desroches, J. Pichette, K. Saint-Arnaud, L. Bernstein, M.-C. Guiot, K. Petrecca, and F. Leblond, "Intraoperative brain cancer detection with Raman spectroscopy in humans," Sci. Transl. Med. **7**, 274–279 (2015).
7. M. H. T. Reinges, H.-H. Nguyen, T. Krings, B.-O. Hütter, V. Rohde, and J. M. Gilsbach, "Course of brain shift during microsurgical resection of supratentorial cerebral lesions: limits of conventional neuronavigation," Acta Neurochir. (Wien) **146**(4), 369–377 (2004).
8. K. A. Ganser, H. Dickhaus, A. Staubert, M. M. Bonsanto, C. R. Wirtz, V. M. Tronnier, and S. Kunze, "Quantification of brain shift effects in MRI images," Biomed. Tech. (Berl.) **42**(s2), 247–248 (1997).
9. D. L. Hill, C. R. Maurer Jr, R. J. Maciunas, J. A. Barwise, J. M. Fitzpatrick, and M. Y. Wang, "Measurement of intraoperative brain surface deformation under a craniotomy," Neurosurgery **43**, 514–528 (1998).

#270836 http://dx.doi.org/10.1364/BOE.7.005129
Journal © 2016 Received 20 Jul 2016; revised 26 Oct 2016; accepted 4 Nov 2016; published 16 Nov 2016

Biomedical Optics EXPRESS

10. A. Nabavi, P. M. Black, D. T. Gering, C. F. Westin, V. Mehta, R. S. Pergolizzi, M. Ferrant, S. K. Warfield, N. Hata, R. B. Schwartz, W. M. Wells, R. Kikinis, and F. A. Jolesz, "Serial intraoperative magnetic resonance imaging of brain shift," Neurosurgery **48**, 787–798 (2001).
11. T. Selbekk, R. Brekken, O. Solheim, S. Lydersen, T. A. N. Hernes, and G. Unsgaard, "Tissue Motion and Strain in the Human Brain Assessed by Intraoperative Ultrasound in Glioma Patients," Ultrasound Med. Biol. **36**(1), 2–10 (2010).
12. M. Jermyn, H. Ghadyani, M. A. Mastanduno, W. Turner, S. C. Davis, H. Dehghani, and B. W. Pogue, "Fast segmentation and high-quality three-dimensional volume mesh creation from medical images for diffuse optical tomography," J. Biomed. Opt. **18**(8), 086007 (2013).
13. H. Dehghani, M. E. Eames, P. K. Yalavarthy, S. C. Davis, S. Srinivasan, C. M. Carpenter, B. W. Pogue, and K. D. Paulsen, "Near infrared optical tomography using NIRFAST: Algorithm for numerical model and image reconstruction," Commun. Numer. Methods Eng. **25**(6), 711–732 (2009).
14. J. Zhao, H. Lui, D. I. McLean, and H. Zeng, "Automated autofluorescence background subtraction algorithm for biomedical Raman spectroscopy," Appl. Spectrosc. **61**(11), 1225–1232 (2007).
15. J. H. Friedman, "Stochastic gradient boosting," Comput. Stat. Data Anal. **38**(4), 367–378 (2002).
16. C. R. Wirtz, F. K. Albert, M. Schwaderer, C. Heuer, A. Staubert, V. M. Tronnier, M. Knauth, and S. Kunze, "The benefit of neuronavigation for neurosurgery analyzed by its impact on glioblastoma surgery," Neurol. Res. **22**(4), 354–360 (2000).
17. N. S. Litofsky, A. M. Bauer, R. S. Kasper, C. M. Sullivan, and O. H. Dabbous; Glioma Outcomes Project Investigators, "Image-guided resection of high-grade glioma: patient selection factors and outcome," Neurosurg. Focus **20**(4), E16 (2006).
18. M. S. Berger, A. V. Deliganis, J. Dobbins, and G. E. Keles, "The effect of extent of resection on recurrence in patients with low grade cerebral hemisphere gliomas," Cancer **74**(6), 1784–1791 (1994).
19. L. Capelle, D. Fontaine, E. Mandonnet, L. Taillandier, J. L. Golmard, L. Bauchet, J. Pallud, P. Peruzzi, M. H. Baron, M. Kujas, J. Guyotat, R. Guillevin, M. Frenay, S. Taillibert, P. Colin, V. Rigau, F. Vandenbos, C. Pinelli, and H. Duffau; French Réseau d'Étude des Gliomes, "Spontaneous and therapeutic prognostic factors in adult hemispheric World Health Organization Grade II gliomas: a series of 1097 cases: clinical article," J. Neurosurg. **118**(6), 1157–1168 (2013).
20. G. E. Keles, K. R. Lamborn, and M. S. Berger, "Low-grade hemispheric gliomas in adults: a critical review of extent of resection as a factor influencing outcome," J. Neurosurg. **95**(5), 735–745 (2001).
21. M. Lacroix, D. Abi-Said, D. R. Fourney, Z. L. Gokaslan, W. Shi, F. DeMonte, F. F. Lang, I. E. McCutcheon, S. J. Hassenbusch, E. Holland, K. Hess, C. Michael, D. Miller, and R. Sawaya, "A multivariate analysis of 416 patients with glioblastoma multiforme: prognosis, extent of resection, and survival," J. Neurosurg. **95**(2), 190–198 (2001).
22. M. J. McGirt, K. L. Chaichana, F. J. Attenello, J. D. Weingart, K. Than, P. C. Burger, A. Olivi, H. Brem, and A. Quinoñes-Hinojosa, "Extent of surgical resection is independently associated with survival in patients with hemispheric infiltrating low-grade gliomas," Neurosurgery **63**, 700–708 (2008).
23. N. Sanai and M. S. Berger, "Glioma extent of resection and its impact on patient outcome," Neurosurgery **62**, 753–764 (2008).
24. I.-F. Talos, K. H. Zou, L. Ohno-Machado, J. G. Bhagwat, R. Kikinis, P. M. Black, and F. A. Jolesz, "Supratentorial low-grade glioma resectability: statistical predictive analysis based on anatomic MR features and tumor characteristics," Radiology **239**(2), 506–513 (2006).
25. C. Ewelt, F. W. Floeth, J. Felsberg, H. J. Steiger, M. Sabel, K.-J. Langen, G. Stoffels, and W. Stummer, "Finding the anaplastic focus in diffuse gliomas: the value of Gd-DTPA enhanced MRI, FET-PET, and intraoperative, ALA-derived tissue fluorescence," Clin. Neurol. Neurosurg. **113**(7), 541–547 (2011).
26. J. Regelsberger, F. Lohmann, K. Helmke, and M. Westphal, "Ultrasound-guided surgery of deep seated brain lesions," Eur. J. Ultrasound **12**(2), 115–121 (2000).
27. N. Sanai, L. A. Snyder, N. J. Honea, S. W. Coons, J. M. Eschbacher, K. A. Smith, and R. F. Spetzler, "Intraoperative confocal microscopy in the visualization of 5-aminolevulinic acid fluorescence in low-grade gliomas," J. Neurosurg. **115**(4), 740–748 (2011).
28. W. Stummer, A. Novotny, H. Stepp, C. Goetz, K. Bise, and H. J. Reulen, "Fluorescence-guided resection of glioblastoma multiforme by using 5-aminolevulinic acid-induced porphyrins: a prospective study in 52 consecutive patients," J. Neurosurg. **93**(6), 1003–1013 (2000).
29. H. J. Böhringer, D. Boller, J. Leppert, U. Knopp, E. Lankenau, E. Reusche, G. Hüttmann, and A. Giese, "Time-domain and spectral-domain optical coherence tomography in the analysis of brain tumor tissue," Lasers Surg. Med. **38**(6), 588–597 (2006).
30. H. J. Böhringer, E. Lankenau, F. Stellmacher, E. Reusche, G. Hüttmann, and A. Giese, "Imaging of human brain tumor tissue by near-infrared laser coherence tomography," Acta Neurochir. (Wien) **151**(5), 507–517 (2009).

1. Introduction

Grade 2-4 gliomas are primary brain cancers that invade into the surrounding normal brain but do not metastasize throughout the body. In contrast to well-circumscribed non-invasive primary brain tumors (grade 1 pilocytic astrocytomas) and secondary brain cancers (metastases), the boundaries of invasive gliomas are not detectable by MRI - the standard of

Biomedical Optics EXPRESS

care imaging modality, intraoperative inspection, or any other technique. Two sets of contemporary data show that residual invasive glioma cells not resected at surgery decrease survival time. i) Eighty-five percent of grade 4 gliomas (glioblastomas) recur at the previous resection cavity margin [1]. ii) The volume of residual cancer is inversely proportional to survival time; patients with no post-operative MRI-detectable contrast-enhancing glioblastoma live more than 3 times longer than patients with greater than 1.5 cm of residual glioblastoma [2]. This inability to detect the entirety of an invasive glioma, in the absence of another suitable biomarker or curative adjuvant therapies, limits the utility of surgical treatment of this non-metastasizing cancer leading to a median recurrence time of 6 months and an overall survival time of 14.6 months [3,4].

With these detection deficiencies in mind, high performance practical optical approaches are being developed for enhanced cancer detection and guidance because of their molecular profiling capabilities [5]. We have shown that Raman spectroscopy (RS), a non-invasive label-free surface imaging modality that gives spectral information based on the vibrational and rotational modes of molecular species in tissue, can detect gliomas during surgery with a sensitivity of 93% and specificity of 91% [6].

Since MRI and existing surgical techniques are not capable of identifying the entirety of a glioma, we compared the invasive glioma sensitivity of MRI versus RS – can RS detect glioma cells that have invaded into the normal brain not detectable by MRI. Specifically, we tested the capability of RS to detect distant invasive glioma cells not detected using T1-contrast-enhanced and T2-weighted MRI sequences in humans during brain cancer surgery. Extending our previous work in which we showed that RS can distinguish brain cancer from normal brain [6], we found that RS is able to intraoperatively detect invasive cancer not detectable using MRI.

2. Methods

2.1 Experimental design for intraoperative Raman spectroscopy

The objective of this study was to investigate the capabilities of Raman spectroscopy (RS) for detecting invasive cancer beyond the signal visible on MRI. RS was used during brain tumor resection for $N = 13$ patients with grade 2-4 gliomas at the Montreal Neurological Institute and Hospital. The study was approved by the Montreal Neurological Institute Ethics Review Board, with informed consent obtained for all patients. The methods were carried out in accordance with the approved guidelines. A hand-held fiber optic probe (EmVision LLC, FL, USA) is connected to a 785 nm laser (Innovative Photonic Solutions, NH, USA) and a high-resolution charge-coupled device spectroscopic detector (ANDOR Technology, Belfast, UK) (Fig. 1). There are seven inelastic scattering (RS) detection optical fibers, one laser excitation fiber, and a PC controls data acquisition with a LabVIEW interface. The diameter of the excitation fiber in the probe is 0.2 mm, and the diameter of the each of the 7 detection fibers is 0.3 mm. A lens is positioned in front of the optical fibers ensuring illumination and detection light paths are such that the tissue excitation area and the detection field-of-view are spatially coincident. The spatial area sampled by the probe is a circular spot size of diameter 0.5 mm and a depth no larger than ~1 mm [6]. The acquired spectra range from Raman shifts of 381 to 1653 cm^{-1}, and the spectral resolution varies between 1.6 and 2.1 cm^{-1}. For each patient, the system was used to measure the Raman spectra at 5-15 locations during surgery. The probe was placed in direct contact with the brain at the resection cavity margin for each measurement, with a total acquisition time of 0.2 s per measurement. This corresponds to three Raman spectra measurements and one background measurement for reference with the excitation laser off. A StealthStation (Medtronic, MN, USA) was used to record the location of each measurement on preoperative MRI scans, by infrared tracking of fiducial markers fixed on the hand-held Raman spectroscopy probe. Superficial biopsy samples were taken at each measurement location for neuropathology analysis.

Biomedical Optics EXPRESS

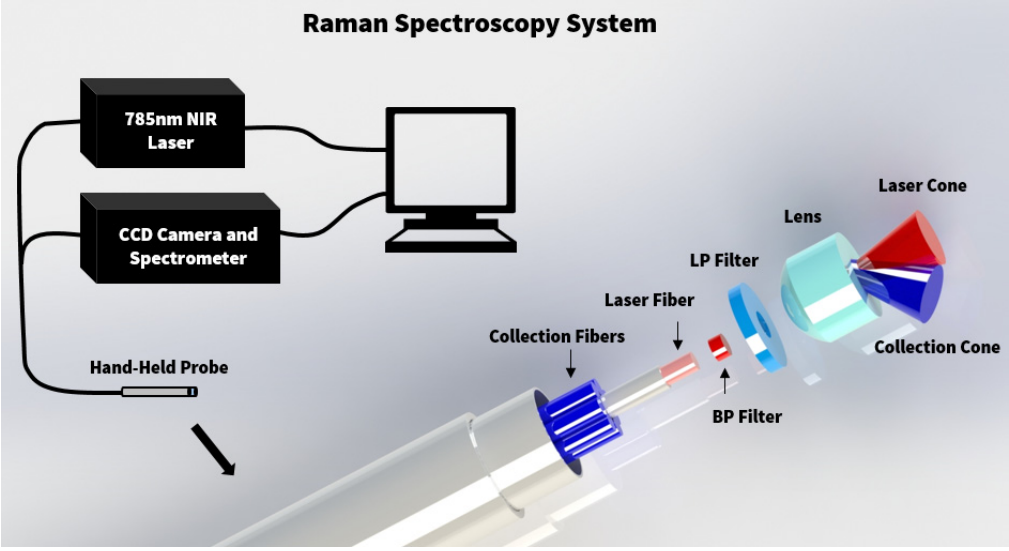

Fig. 1. Experimental setup diagram with the hand-held fiber optic Raman probe connected to a 785 nm NIR laser and high-resolution CCD spectroscopic detector.

2.2 Neuropathological assessment

Neuropathological analysis was performed by M.C.G., a neuropathologist with expertise in neuro-oncology. Cancer cells were identified on hematoxylin and eosin (H&E) stained sections. Cell counting was performed on H&E stained images to determine the cancer cell count per area. IDH1 (R132H) immunohistochemistry was also used to complement the H&E staining for cancer cell identification [6] (Fig. 2).

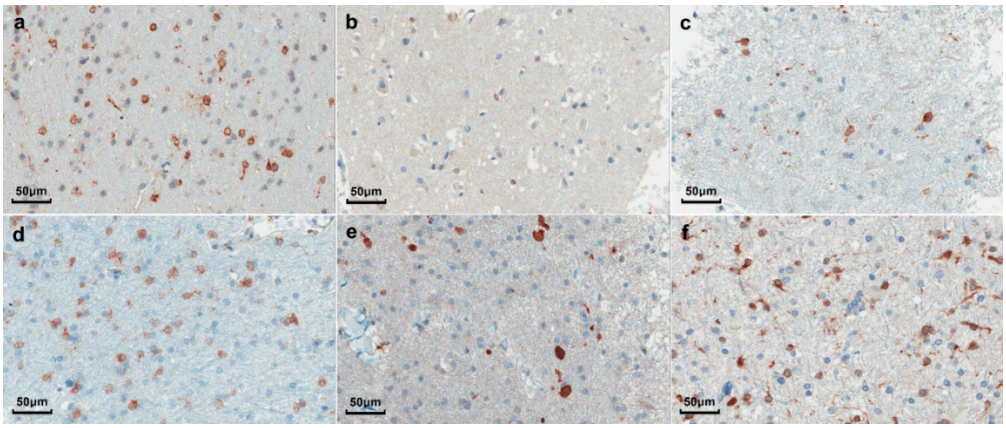

Fig. 2. Images of neuropathology slides from tumor samples for 6 patients mutated for IDHR132H, corresponding to: **(a)** Anaplastic Astrocytoma (WHO grade 3); **(b)** Recurrent Oligodendroglioma (WHO grade 2); **(c)** Recurrent Astrocytoma (WHO grade 2); **(d)** Anaplastic Oligodendroglioma (WHO grade 3); **(e)** Anaplastic Astrocytoma (WHO grade 3); **(f)** Glioblastoma (WHO grade 4).

2.3 Brain shift correction

The comparison of visible tumor on preoperative MRI with RS measurement locations can be potentially affected by brain shift during surgery [7–9]. In order to minimize the effects of spatial registration errors, landmark locations were recorded during surgery on the cortical surface. These landmarks were compared with a reconstructed cortical surface from

Biomedical Optics EXPRESS

segmented MR images in order to estimate brain shift. Moreover, the areas sampled in this study were primarily by white matter tracts near the midline which typically do not shift during surgery [9–11]. These areas are reinforced structurally by the fixed and rigid falx membrane that separates hemispheres. This diminishes any motion artifacts which may hinder neuronavigation. Moreover, the surgeon ensures that excess blood, water, or CSF is drained and/or regulated and samples are measured on relaxed intact tissue. Intracranial pressure and pulsatility are reduced, and the straining effect due to cerebral blood flow and brain swelling is diminished in tumor-invasive tissue.

2.4 Tumor segmentation on preoperative MRI

The preoperative MRIs were used to determine the boundary limits of cancer visible on T1-contrast enhanced and T2-weighted sequences. All image processing was performed using the medical image segmentation and visualization tools in NIRFAST [12,13]. Semi-automated segmentation algorithms were used to identify the tumor region on MR images, and manual manipulation of the segmentation was used to further refine the result. While the exact segmentation process varied across patients due to differences in contrast and tumor structure, a description of the typical workflow for segmenting the tumor region follows. Figure 3 shows an example of each step of the segmentation process. The MRI volume was first cropped down to the area around the tumor. Then a K-means and Markov random field algorithm was used to identify areas of similar grayscale values and structure in the remaining MRI volume (see the blue, yellow, and red regions in Fig. 3). The resulting region most accurately delineating the tumor area was kept, and all other regions discarded. A connected component algorithm was used to remove noise away from the tumor area. Iterative label hole filling was then used to remove any small holes in the segmentation. Finally, each slice of the MRI volume was examined to ensure that the segmentation identified all hyperintense regions of the tumor, with manual manipulation used to correct any errors in segmentation. Detailed descriptions of the segmentation algorithms can be found in previous work [12]. Segmentation was independently verified by Kevin Petrecca (neurosurgeon) and Mariam Alrashid (neurosurgeon). The measurement locations for RS were co-located on the T1- and T2-weighted MRI, which allowed for a comparison of the relative distance of these locations from the tumor segmentations.

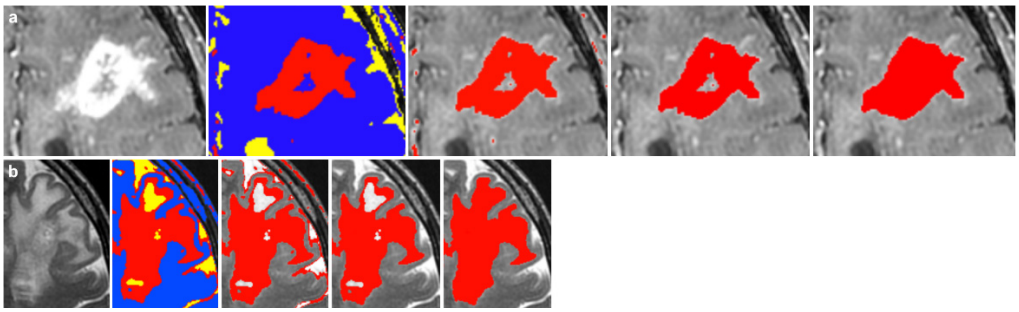

Fig. 3. This example shows the segmentation of a glioblastoma on T1-contrast enhanced **(a)** and T2-weighted **(b)** MRI. After cropping the MRI volume to the tumor area, semi-automated segmentation algorithms use grayscale values and structure to identify MR-enhancing areas corresponding to tumor. The final step (far right) shows the resulting tumor segmentation in red.

2.5 Pre-processing and analysis of Raman spectroscopy data

All spectra were pre-processed to subtract background reference spectra, normalize for laser power, and remove intrinsic tissue fluorescence using an iterative polynomial fit [14]. The boosted trees supervised machine learning algorithm was used to distinguish the spectra of all cancer tissue from normal brain. The algorithm uses an ensemble of decision trees based on

Biomedical Optics EXPRESS

training data to distinguish tissue types [15]. In the present work we are considering only the samples of normal brain and of invasive cancer. Namely, out of a total 128 measurements made for the N = 13 patients, only those associated with locations of normal brain (45 measurements) or invasive cancer (60 measurements) were used. Samples were labelled invasive cancer if they had ≤90% cancer cells present. The classifier was used to distinguish the invasive cancer samples presented here from normal brain using leave-one-out cross-validation. The total time for pre-processing and classification of a Raman spectrum was measured to be 0.068 s on a PC with an Intel i7-3770 CPU (3.40 GHz). Statistical analysis on classification accuracy was performed using two-sided normal-based 95% confidence intervals. Table 1 provides sample size and histological diagnosis for the patients.

Table 1. Patient pathology and sample size information: A total of 60 invasive cancer samples were used, with a further 45 measurements of normal brain.

		***N* patients**	***n* samples**
WHO grade 2		**2**	**4**
	Astrocytoma	1	2
	Oligodendroglioma	1	2
WHO grade 3		**4**	**12**
	Astrocytoma	2	5
	Oligodendroglioma	1	1
	Oligoastrocytoma	1	6
WHO grade 4	**Glioblastoma**	**7**	**44**
Total		**13**	**60**

3. Results

3.1 Intraoperative Raman spectroscopy during brain tumor resection

The capability of RS to detect brain cancer cells that had invaded into the brain beyond the detection capability of MRI was assessed in thirteen patients with invasive grade 2-4 glioma. Surgical planning MRI data from each patient was used for 3-dimensional surgical navigational guidance [16,17] with a StealthStation navigation unit (Medtronic MN, USA). Surgeries were performed using standard microsurgical techniques. During surgery the suspected glioma boundary limits were identified based on navigational guidance, visual tissue properties, and tactile sensation of the tissue. Raman spectra were obtained at discrete points in these areas using the hand-held probe (*Methods*) in contact with tissue, with a circular laser spot of diameter 0.5 mm. The tissue at each interrogated point was collected and archived for post-surgical blinded neuropathological analysis (Table 1). These sites were also landmarked using the navigation system to allow for a direct comparison of the RS signal obtained versus the MRI signal at each site (Fig. 4(b)).

Biomedical Optics EXPRESS

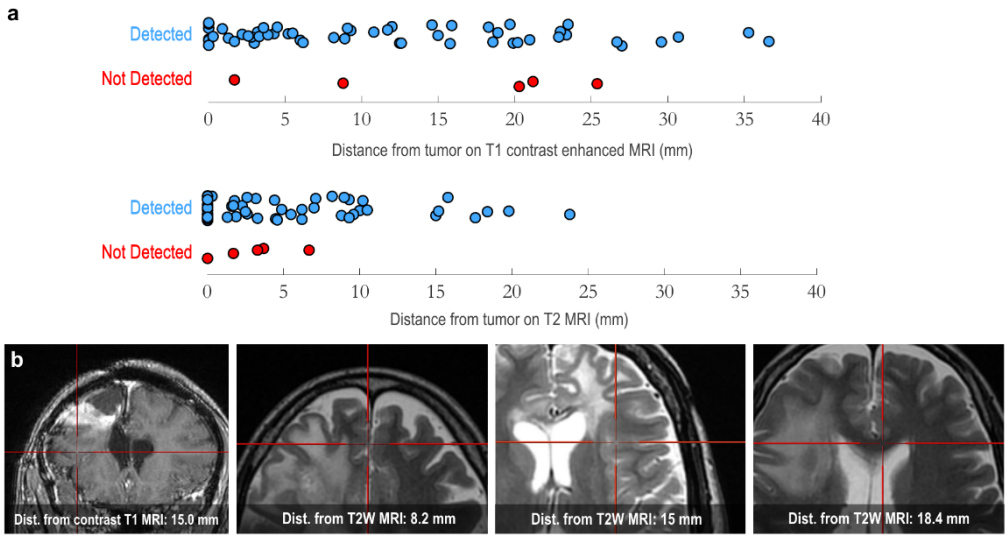

Fig. 4. (a) Three-dimensional distances of invasive cancer samples (13 patients, n = 60 tissue samples) from the closest edge of visible tumor contrast on preoperative T1-contrast enhanced (top) and T2-weighted (bottom) MRI. The location of the invasive cancer samples was determined on preoperative MRI based on the StealthStation tracking system used during surgery. 'Detected' versus 'Not Detected' indicates which samples the classification algorithm was able to correctly identify as invasive cancer based on RS (true positive), and those which where misclassified (false negative), respectively. Note that the vertical axis is used only to provide separation of the data points to make the points with similar values on the horizontal axis more visible. (b) MRI images (from different patients) showing four sample RS measurement locations indicated by the red cross-hair: one coronal T1-contrast enhanced image for a patient with grade 3 anaplastic astrocytoma (left), followed by three axial T2-weighted images, corresponding to patients with grade 4 glioblastoma, grade 3 anaplastic astrocytoma, and grade 4 glioblastoma, respectively. For each, the three-dimensional distance of the measurement location from T1-contrast enhanced or T2-weighted MRI contrast respectively is indicated.

3.2 MRI tumor segmentation and neuronavigation

To determine the relationship between the RS signal and the MRI signal representing glioma we reconstructed the MRI signal corresponding to the tumor in 3D within the brain using semi-automated segmentation algorithms. This technique generates a true correspondence between the T2-weighted and T1-contrast enhanced signals and the segmentation (Fig. 3). For each RS site interrogated the distance from that site and the nearest abnormal MRI signal obtained from the 3D cancer segmentations was calculated. As an example, Figs. 5(b)-5(e) shows the segmented tumor region for a patient with a glioblastoma on T1-contrast enhanced and T2-weighted MRI. The locations of the RS measurements for invasive cancer are shown relative to the tumor segmentations in Fig. 5(a).

Biomedical Optics EXPRESS

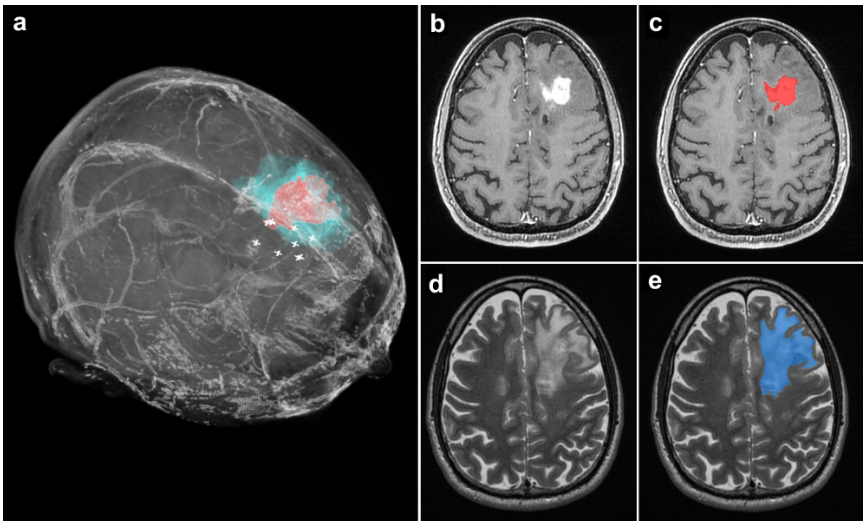

Fig. 5. (a) 3-Dimensional volume rendering from the preoperative MRI of a patient with a grade 4 glioblastoma. The tumor regions visible on T1- and T2-weighted MRI scans are indicated in red and blue respectively. White 'plus' symbols indicate measurement locations of invasive cancer detected with RS. (b) A T1-weighted MR axial image with the glioblastoma visible. (c) The same image as in b, with the segmentation of the tumor region visible in red. (d) A T2-weighted MR axial image with the glioblastoma visible, corresponding to the same cross section as in b and c. (e) The same image as in d, with the segmentation of the tumor region visible in blue.

3.3 Raman spectroscopy tissue classification

A supervised machine learning boosted trees classification algorithm [15] that utilizes all spectral data, rather than relying on specific spectral bands, was used to distinguish samples containing invasive cancer cells versus normal brain. We found that RS is able to detect distant invasive cancer cells up to ~3.7 cm beyond the T1-contrast enhanced MRI boundary and up to ~2.4 cm beyond the T2 MRI boundary (Fig. 4(a), $N = 13$ patients, $n = 60$ invasive cancer tissue samples). RS was able to detect invasive cancer with 92% accuracy, 92% sensitivity, and 93% specificity (two-sided normal-based 95% confidence intervals of $< \pm$ 5%). The false negative rate was 8%, and the false positive rate was 7%. The corresponding RS signal and histopathology is shown in Fig. 6 for interrogated sites. Note that instrument response was not removed from the Raman spectra, and so several of the low-frequency features visible in the spectra will be associated with instrument response (especially associated with long-pass filters). This does not affect the ability to classify tissue using machine learning, since the instrument response is consistent throughout all measurements which were made with the same instrument. In this study we found that RS can detect as few as 6 cancer cells per 0.0625 mm^2.

Biomedical Optics EXPRESS

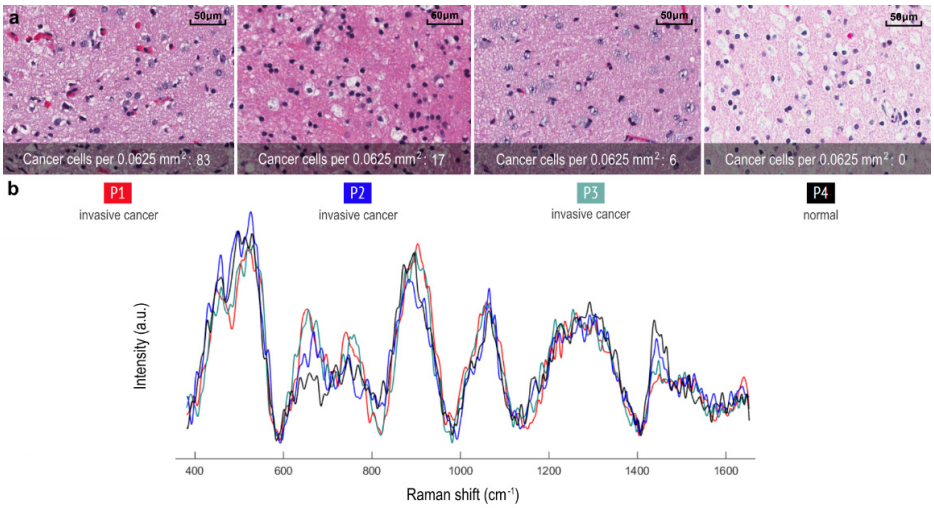

Fig. 6. (a) Histopathology images for 4 tissue samples are shown: Three invasive grade 4 glioblastoma samples and one normal brain sample from a patient with a grade 2 astrocytoma, corresponding to locations where RS were made. (b) Raman spectra of the measurement locations in **a**, with visible spectral differences.

4. Discussion

The appreciation that current imaging technologies, including standard of care MRI, cannot detect distant invasive brain cancer cells is critical because this limitation profoundly reduces the effectiveness of the surgical treatment of glioma. In fact this concept has been acknowledged for decades yet no substantial advances have been made [1,18–24]. Here, we demonstrate that RS can detect invasive cancer cells well beyond cancer detected on MRI in humans during surgery. RS detects invasive cancer up to ~3.7 cm and ~2.4 cm beyond T1-contrast enhanced and T2 MRI boundary, respectively.

This RS system is ideal for intraoperative glioma detection. It has a small footprint, rapid acquisition time, and is highly accurate. It can detect invasive cancer cells without disrupting the neurosurgical workflow and could complement or replace MRI-guided neuronavigation as a technique to identify cancer margins. This has potential to function as an intraoperative guide during brain cancer surgery, minimizing the number of cancer cells remaining following surgery. Imaging modalities such as positron emission tomography (PET), ultrasound (US), fluorescence-guided imaging, and optical coherence tomography (OCT) have been used for the detection of brain cancer, but with limited sensitivity and specificity for low-grade gliomas and invasive cancer [25–30]. Considering that 85% of glioblastomas recur at the previous resection cavity margin, RS-guided invasive cancer cell detection may increase the effectiveness of surgery and directly lengthen patient survival.

Funding

Fonds de recherché du Quebec – Nature et technologies (FRQNT); Natural Sciences and Engineering Research Council of Canada (NSERC); Canadian Institutes of Health Research (CIHR); Groupe de Recherche en Sciences et Technologies (GRSTB); Banque Nationale.

Acknowledgements

K.P and F.L are co-founders of ODS Medical Inc, a medical device company that seeks to commercialize the Raman spectroscopy system for real-time detection of tissue abnormalities. Kelvin Mok assisted with neuronavigation techniques. Mariam Alrashid provided independent assessment of MRI tumor segmentation.